Mon. Not. R. Astron. Soc. **000**, 000–000 (0000) Printed 7 January 2016 (MN LATEX style file v2.2)

Mapping kiloparsec-scale structures in the extended H I disc of the galaxy UGC 000439 by H I 21-cm absorption

R. Dutta[1⋆], N. Gupta[1], R. Srianand[1], J. M. O'Meara[2]
[1] *Inter-University Centre for Astronomy and Astrophysics, Post Bag 4, Ganeshkhind, Pune 411007, India*
[2] *Department of Chemistry and Physics, Saint Michael's College, One Winooski Park, Colchester, VT 05439, USA*

Accepted. Received; in original form

ABSTRACT

We study the properties of H I gas in the outer regions ($\sim 2r_{25}$) of a spiral galaxy, UGC 00439 (z = 0.01769), using H I 21-cm absorption towards different components of an extended background radio source, J0041−0043 (z = 1.679). The radio source exhibits a compact core coincident with the optical quasar and two lobes separated by ∼7 kpc, all at an impact parameter ∼25 kpc. The H I 21-cm absorption detected towards the southern lobe is found to extend over ∼2 kpc^2. The absorbing gas shows sub-kpc-scale structures with the line-of-sight velocities dominated by turbulent motions. Much larger optical depth variations over 4-7 kpc-scale are revealed by the non-detection of H I 21-cm absorption towards the radio core and the northern lobe, and the detection of Na I and Ca II absorption towards the quasar. This could reflect a patchy distribution of cold gas in the extended H I disc. We also detect H I 21-cm emission from UGC 00439 and two other galaxies within ∼150 kpc to it, that probably form an interacting group. However, no H I 21-cm emission from the absorbing gas is detected. Assuming a linear extent of ∼4 kpc, as required to cover both the core and the southern lobe, we constrain the spin temperature $\lesssim 300$ K for the absorbing gas. The kinematics of the gas and the lack of signatures of any ongoing *in situ* star formation are consistent with the absorbing gas being at the kinematical minor axis and corotating with the galaxy. Deeper H I 21-cm observations would help to map in greater detail both the large- and small-scale structures in the H I gas associated with UGC 00439.

Key words: galaxies: individual: UGC 00439, UGC 00435 and CGCG 383−072 − galaxies: ISM − quasars: absorption line − quasars: individual: UM 266.

1 INTRODUCTION

In multiphase pressure equilibrium models, as well as supernova driven hydrodynamical simulations, the physical conditions, volume filling factors and pc- to kpc-scale structures of different phases of H I gas in the interstellar medium (ISM) of galaxies are found to depend on various radiative and mechanical feedback processes associated with the *in situ* star formation (McKee & Ostriker 1977; Wolfire et al. 1995; de Avillez & Breitschwerdt 2004; Gent et al. 2013; Gatto et al. 2015). Therefore, understanding the properties of H I gas phases, especially the cold neutral medium (CNM) which is closely related to the molecular gas, is crucial to understand processes through which gas gets converted to stars.

In our Galaxy, H I 21-cm emission and absorption line observations have been extensively used to characterize physical conditions and pc- to kpc-scale structures in the ISM (Heiles 1984; Frail et al. 1994; Deshpande 2000; Heiles & Troland 2003; Brogan et al. 2005). Since H I 21-cm absorption is sensitive to the spin temperature (T_s), which is coupled to the kinetic temperature of the gas (Roy et al. 2006), repeated measurements of H I 21-cm absorption towards high-velocity pulsars, extended radio sources, and radio sources with jets having proper motion, have been particularly useful in revealing small-scale structures of CNM. However, due to the scarcity of known strong and extended radio sources at close impact parameters with respect to galaxies, it has been possible to extend such studies to very few external galaxies (see Wolfe et al. 1982; Briggs et al. 2001; Kanekar & Chengalur 2001, 2005; Srianand et al. 2013). H I 21-cm emission line observations of nearby dwarf and spiral galaxies show that the properties of CNM and warm neutral medium (WNM) and ∼100 pc- to 2 kpc-scale structures detected in the H I gas are coupled to the local star formation in galaxies (e.g. Tamburro et al. 2009; Bagetakos et al. 2011; Ianjamasimanana et al. 2012). However, in the absence of absorption line measurements it is not known whether the H I 21-cm emission line components exhibiting smaller line widths (and hence assumed to correspond to CNM) are truly cold. Therefore,

⋆ E-mail: rdutta@iucaa.in

the contributions due to turbulent motions and the processes driving the observed properties of H I gas are poorly constrained.

In this paper, we present results from H I 21-cm absorption and emission line observations of a low-z Quasar-galaxy-pair (QGP)[1], discovered through our ongoing efforts to characterize the cold atomic gas phase around low-z galaxies (Gupta et al. 2010, 2013; Srianand et al. 2013; Dutta et al. 2015; Srianand et al. 2015). This QGP consists of a radio-loud quasar (QSO), J0041−0143 (J004126.01−014315.6, also known as UM 266; $z_{\rm em}$ = 1.679), at an impact parameter (b) ∼25 kpc from the spiral galaxy, UGC 00439 (J004121.53−014257.0; z_g = 0.0177). This QGP is special in three regards. First, the background radio source shows multiple components spread over few arcseconds. J0041−0143 consists of a radio core component and two lobes spread over ∼ 20″ in the 1.4 GHz continuum map (Downes et al. 1986), with the structures resolving into compact clumps in the higher frequency maps (Barthel et al. 1988; Fernini 2014, 5 GHz and 8.4 GHz respectively). High continuum flux of individual components provides us with the unique opportunity to use H I 21-cm absorption to probe the distribution and structure of the CNM gas up to ∼7 kpc at the redshift of the foreground galaxy. Secondly, the radio source is located well outside the optical stellar disc of UGC 00439, allowing us to probe conditions in the extended H I disc. Finally, the foreground galaxy is close enough to detect H I 21-cm emission and carry out a joint H I 21-cm emission/absorption line analysis to address some of the above mentioned issues. Till date about 12 low-z H I 21-cm absorbers have been detected from the observations of QGPs (see Carilli & van Gorkom 1992; Borthakur et al. 2010, 2011; Reeves et al. 2015; Zwaan et al. 2015, in addition to the above mentioned studies of QGPs). Most of these are associated with the stellar discs of late-type galaxies and are towards quasars with radio emission compact at kpc scales, and joint analysis of absorption and emission measurements have been performed in very few cases (see Stocke et al. 1991, 2010; Keeney et al. 2005, 2011).

This paper is structured as follows. In Section 2, we summarize various properties of the host galaxy, UGC 00439, as provided in the literature. In Section 3, we describe our Giant Metrewave Radio Telescope (GMRT) observations of the system. Next, we give details of the GMRT H I 21-cm absorption towards the background radio source, of the GMRT H I 21-cm emission from the galaxy, and of the metal absorption lines detected in the optical spectrum of the QSO obtained using the Keck High Resolution Echelle Spectrometer (HIRES), in Section 4. We then discuss the origin of the H I 21-cm absorber in terms of the host galaxy properties in Section 5. We conclude by summarizing our results in Section 6. Throughout this work we have adopted a flat cosmology with H_0 = 70 km s^{-1} Mpc^{-1} and Ω_m = 0.27.

2 PROPERTIES OF UGC 00439

The galaxy, UGC 00439, is part of the Near Field Galaxy Survey (Jansen et al. 2000b,a), which provides the U-, B-, R-band integrated and nuclear spectrophotometry. In B-band, UGC 00439 has an absolute magnitude, $M_B \sim -20.6$, luminosity, log L_B ∼10.4 $L_\odot$, and radius at which the surface brightness drops to 25 mag arcsec^{-2}, r_{25}^B ∼36″ (13 kpc). From the optical photometry, UGC 00439 is classified as a face-on (inclination angle, i = 0°) Sa galaxy having a position angle (PA) of the major axis (measured north through east) of 170°. However, from the Two Micron All-Sky Survey (2MASS) K_s band photometry, UGC 00439 is estimated to have i = 31° and PA of major axis = 160° (Skrutskie et al. 2006). UGC 00439 is a star-forming (integrated SFR(Hα) ∼5 $M_\odot\ yr^{-1}$) galaxy with solar metallicity (log(O/H) + 12 ∼8.9) (see for details Kewley et al. 2004). Kannappan et al. (2013) estimated the stellar mass of UGC 00439 as, log M_* ∼10.5 $M_\odot$. From the correlation found between the optical B-band magnitude and the H I size of low-z galaxies (Broeils & Rhee 1997; Lah et al. 2009), the diameter within which half the H I mass of the galaxy is expected to be contained is ∼28 kpc. The Arecibo single dish H I 21-cm emission spectrum of the galaxy gives the velocity width of the emission as 115 ± 2 km s^{-1} and the total integrated flux density as, $\int Sdv$ = 7.07 ± 0.76 Jy km s^{-1} (Springob et al. 2005). This total flux density translates into an H I mass, log M(H I) = 9.99 ± 0.05 $M_\odot$. The H I 21-cm, optical and ultraviolet (UV) observations in the literature of UGC 00439 satisfy the standard scaling relations obtained from the Arecibo Legacy Fast Arecibo L-band Feed Array (α.40), Sloan Digital Sky Survey (SDSS) and Galaxy Evolution Explorer (GALEX) surveys (Huang et al. 2012). The optical spectra of the nuclear region of the galaxy from the Six-degree-Field Galaxy Survey (Jones et al. 2009) gives its redshift as z = 0.017694 ± 0.000150 (heliocentric velocity, $V_{\rm H}$ = 5304.5 ± 45 km s^{-1}), which matches well with that obtained from the Arecibo H I 21-cm emission (z = 0.017686 ± 0.000005 and $V_{\rm H}$ = 5302 ± 2 km s^{-1}).

3 RADIO OBSERVATIONS

The QSO J0041−0143 was observed twice using the GMRT on 2014 October 17 (2.6h on source) and 2015 July 4 (4.5h on source). The observing setup for the first run was optimized to detect H I 21-cm absorption at the redshift of the foreground galaxy, UGC 00439, using a baseband bandwidth of 4.17 MHz split into 512 channels (velocity resolution ∼1.8 km s^{-1}). Whereas in the second run, we used maximum available bandwidth to cover the H I 21-cm emission associated with UGC 00439, i.e. a baseband bandwidth of 16.67 MHz split into 512 channels (velocity resolution ∼7.1 km s^{-1}). In both observations the pointing centre was at RA = $00^h41^m26.01^s$, Dec = −01°43′15.59″ (J2000), and the band was centred on the redshifted H I 21-cm frequency of UGC 00439. Standard calibrators were regularly observed during both the observations for flux density, bandpass, and phase calibrations. The data were reduced using the National Radio Astronomy Observatory (NRAO) Astronomical Image Processing System (`AIPS`) following standard procedures as in Gupta et al. (2010). After initial flagging and gain calibration, a continuum map of the target source was made excluding channels at the edge and the centre of the band where the emission/absorption is expected. Using this map as a model, self-calibration complex gains were determined which were also applied to all the frequency channels. The self-calibrated continuum map was used to subtract the continuum emission from the visibility data set using the `AIPS` task `'UVSUB'`. Then the heliocentric correction was applied to the visibility data set using the `AIPS` task `'CVEL'`. The analyses of H I 21-cm absorption towards J0041−0143 as described in Sections 4.1, 4.2 and 4.3 is based on the data of 2014 October 17, and the analyses of H I 21-cm emission from UGC 00439 as described in Section 4.5 is based on the data of 2015 July 4. The continuum subtracted visibility data sets from these were subjected to imaging with appropriate weightings to detect the H I 21-cm absorption and emission. Details of the

[1] Quasar sightlines passing through discs/haloes of foreground galaxies.

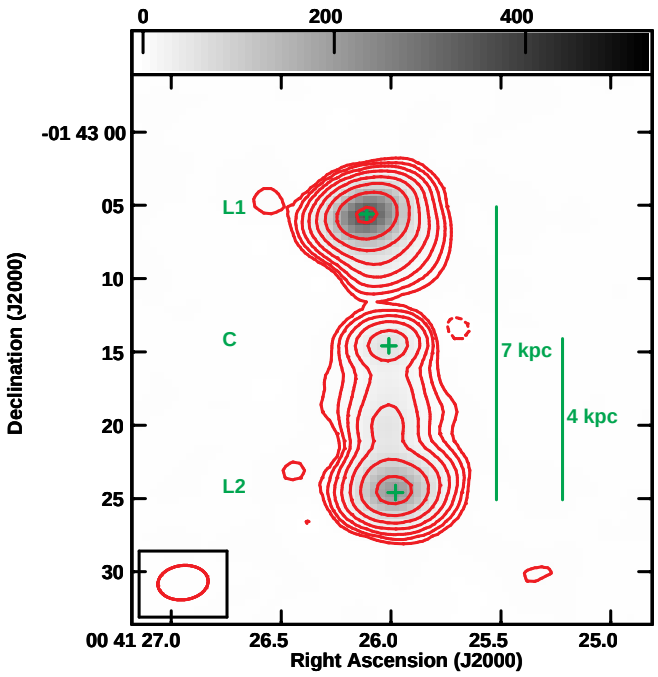

Figure 1. GMRT image of J0041−0143 at 1.4 GHz. The contour levels are plotted as $2.5 \times (-1,1,2,4,8,...)$ mJy beam^{-1}. Note that solid lines correspond to positive values while dashed lines correspond to negative values. At the bottom left corner of the image the restoring beam is shown as an ellipse. The size and PA of the beam are $3.44'' \times 2.34''$ and $-83.60°$ respectively. The continuum peaks of the core, the northern lobe and the southern lobe are identified as C, L1 and L2 respectively. The vertical lines indicate the projected separation between these components at the redshift of UGC 00439.

imaging parameters and properties of the images are described in the following sections.

4 ANALYSES

4.1 Radio continuum of J0041−0143

The radio source, J0041−0143, in our GMRT continuum image (see Fig. 1), consists of a core co-spatial with the optical QSO and two lobes separated by $\sim 20''$. The continuum image, made using `ROBUST=0` weighting and no *uv*-taper in the `AIPS` task `'IMAGR'`, is of spatial resolution $3.44'' \times 2.34''$, and has root mean square noise (rms) of 0.5 mJy beam^{-1} near the target source and rms of 0.2 mJy beam^{-1} away from it. The integrated flux density of the radio source in our image is 1026 mJy, consistent with that reported in the Faint Images of the Radio Sky at Twenty-Centimeters (FIRST; 1040 mJy) and the NRAO VLA Sky Survey (NVSS; 1034 mJy) catalogs. Note that the higher spatial resolution of the GMRT image, as compared to that of FIRST ($\sim 5''$) and NVSS ($\sim 45''$), allows us to resolve all the three radio components distinctly. The radio 'core', i.e. the component coincident with the optical QSO, and the radio continuum peaks associated with the northern and the southern lobes are labelled as C, and L1 and L2 respectively.

4.2 H I 21-cm absorption towards J0041−0143

The continuum-subtracted data set was imaged using the same weighting and beam as the `ROBUST=0` continuum image described above (and shown in Fig. 1). Due to the lack of short baselines which were affected by radio frequency interference and flagged, and the choice of `ROBUST=0` weighting, no H I 21-cm emission was detected in the cube. For deconvolution of H I 21-cm absorption signal while imaging the continuum-subtracted visibility data set in the `AIPS` task `'IMAGR'`, a mask true only for pixels >2.5 mJy beam^{-1} in the radio continuum image (Fig. 1) was used. The final image cube has rms $\sim$2.0 mJy beam^{-1} channel^{-1}. The spectra at the location of the radio components of interest were extracted from this cube, and if necessary, a first-order cubic spline was fitted to remove the residual continuum from the spectra.

We detect H I 21-cm absorption towards L2 at the systematic redshift of UGC 00439, with a maximum line depth of 16 mJy (i.e. at 8σ significance). The H I 21-cm absorption towards L2 is spread over 10 channels or $\sim$18 km s^{-1}, with peak optical depth, τ_p = 0.08 $\pm$ 0.01, and total integrated optical depth, $\int \tau dv$ = 0.52 $\pm$ 0.07 km s^{-1}. However, we do not detect any H I 21-cm absorption towards L1 or C. The optical depth towards L1 and C has to be less than that towards L2 by a factor of $\gtrsim$7 and of $\gtrsim$2 respectively (at 3σ level). The H I 21-cm absorption spectra towards L1, C and L2 are shown in Fig. 2, while the parameters derived from these spectra are provided in Table 1.

The H I 21-cm absorption profile towards L2 shows a clear evidence of arising from the CNM phase. Although the CNM phase is observed to exhibit a range of temperatures ($\sim$20−200 K), for the sake of simplicity we adopt throughout this paper a typical CNM mean temperature of 100 K, as observed in the Milky Way (Heiles & Troland 2003), to infer the physical nature of the H I 21-cm absorption component. In the absence of subarcsecond-scale spectroscopic observations, we assume unit covering factor (f_c) of the cold H I absorbing gas within the beam. The H I 21-cm optical depth towards L2 translates to a column density of H I gas in the CNM phase of $9.5 \times 10^{19} \times (T_s/100\ \mathrm{K})(1/f_c)\,\mathrm{cm}^{-2}$ (see Table 1). The H I 21-cm optical depth constraints towards L1 and C lead to $N(\mathrm{H\,I}) < 1.3 \times 10^{19} \times (T_s/100\ \mathrm{K})(1/f_c)\,\mathrm{cm}^{-2}$ and $N(\mathrm{H\,I}) < 5.1 \times 10^{19} \times (T_s/100\ \mathrm{K})(1/f_c)\,\mathrm{cm}^{-2}$ in the CNM phase respectively.

A single Gaussian is adequate to fit the H I 21-cm absorption line detected towards L2. The best-fitting Gaussian to the H I 21-cm absorption line (as shown in Fig. 2) has a full width at half-maximum, FWHM = 8 $\pm$ 1 km s^{-1}. This constrains the kinetic temperature as $\leqslant$1400 K. In nearby spiral galaxies, CNM and WNM phases have been identified through decomposition of H I 21-cm emission lines into narrow (average dispersion, $\sigma \sim$7 km s^{-1}) and broad ($\sigma \sim$17 km s^{-1}) components (Tamburro et al. 2009). The average dispersion of the narrow component observed in these galaxies at $r \sim 2r_{25}$ (i.e. similar to the J0041−0043 - UGC 00439 impact parameter) is $\sim$6 km s^{-1} (FWHM $\sim$14 km s^{-1}) implying $T \leqslant$4300 K. Thus, it appears that in the outer discs of galaxies, the thermal broadening is much less effective than the turbulence in the gas. We come back to this point in Section 4.3.

4.3 Extent and structure of H I 21-cm absorbing gas

The extended nature of the background radio source allows us to study the spatial extent and structure of the gas giving rise to the H I 21-cm absorption. As indicated above, the absorbing gas may extend up to the core ($\sim$3.6 kpc from L2) of J0041−0143, with

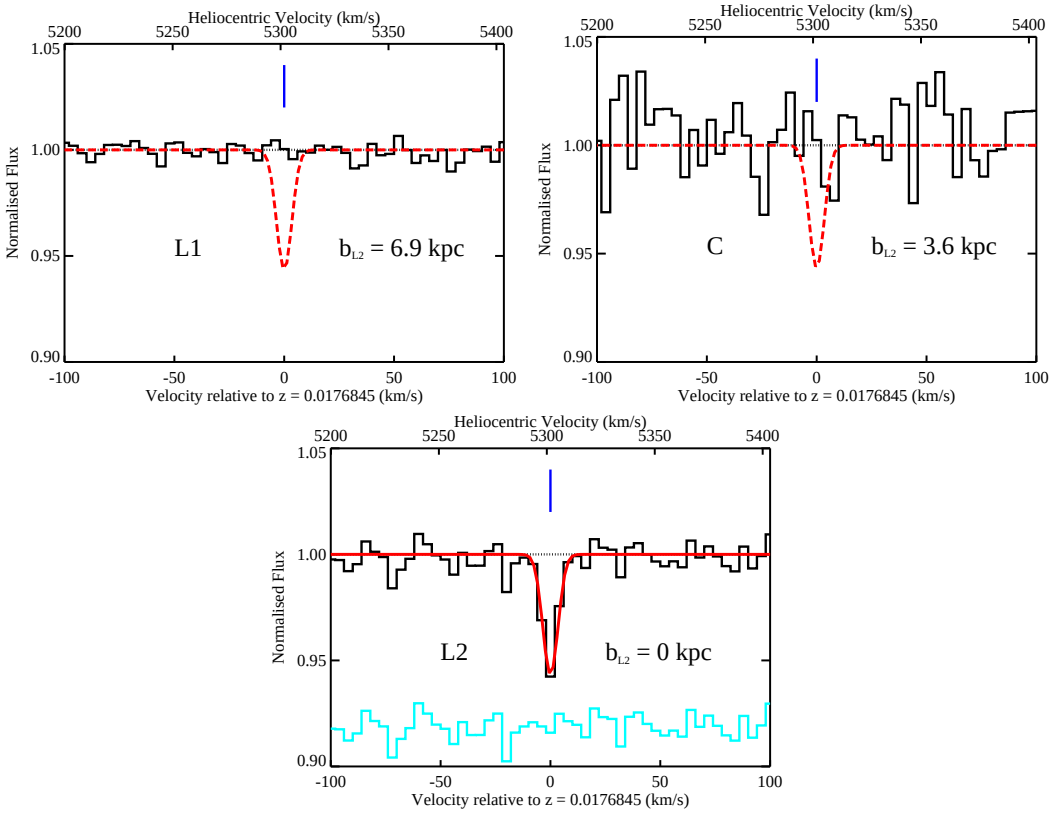

Figure 2. GMRT H I 21-cm absorption spectra towards the continuum components L1 *(Top Left)*, C *(Top Right)* and L2 *(Bottom)*, as marked in Fig. 1. The spectra are smoothed to 4 km s^{-1} for display purpose. In the bottom panel the best-fitting single Gaussian profile to the H I 21-cm absorption towards L2 is overplotted in solid red line, and the residuals from the fit (shifted in the flux scale for display) are plotted below in cyan. This fit is also overplotted in the other two panels in dashed red line for comparison. The vertical tick marks the position of the peak optical depth detected towards L2. b_{L2} given in each panel is the projected separation of the background continuum emission with respect to L2 at the redshift of UGC 00439, as also indicated in Fig. 1.

optical depth dropping by a factor of $\gtrsim$2 between the lines-of-sight towards L2 and C. However, it is unlikely to extend up to the northern lobe ($\sim$7 kpc from L2) since the optical depth towards L1 is at least factor of 7 less than that towards L2. In Fig. 3, we show the channel maps of the H I 21-cm absorption detected towards the southern lobe (dashed contours), overlaid on the continuum contours of J0041−0143 for reference. The H I 21-cm absorption is detected at a significance of $\geqslant 3\sigma$ over 4 channels or 7.2 km s^{-1}. From Fig. 3, we can see that the H I 21-cm absorption has an extended structure, and is spread over a region larger than that of the beam (i.e. $\gtrsim$ 1 kpc^2) in two channels (having $V_{\rm H}$ = 5299 km s^{-1} and 5303 km s^{-1} respectively). To check the spatial extent of the absorbing gas we extracted spectra towards different sightlines separated by the beam size in the southern lobe. In Fig. 4 we show the H I 21-cm absorption spectra towards four such sightlines where H I 21-cm absorption is detected at $\geqslant 2\sigma$, and their details are provided in Table 1. The spatially resolved extraction seems to indicate that the absorption is likely to extend up to $\sim$2 kpc^2, covering most of the southern lobe. Note that we have checked that all the absorption features are present in both the XX and YY polarization spectra for consistency. However, we caution that the optical depth sensitivity falls off rapidly away from L2, and the H I 21-cm absorption towards these sightlines are at lower levels of significance ($\sim$2-3σ).

In addition, from Fig. 3, we note that the location of the maximum absorption or optical depth does not always coincide with that of the peak radio continuum flux. This can be caused by the radio emission in the southern lobe resolving into structures at sub-kpc-scales, as indicated by the 5 GHz (Barthel et al. 1988) and the 8.4 GHz (Fernini 2014) continuum maps of this source. However, it is interesting to note from this figure that the location of the maximum absorption shifts with velocity. From two-dimensional single component Gaussian fitting to the absorption, we find that the centre of the absorption shifts by 1″ over 5.4 km s^{-1}. This seems to indicate that the absorbing gas itself has structures at sub-kpc-scales and a line-of-sight velocity dispersion of the order of few km s^{-1}. This is further reflected in the variation (by factor $\sim$3) seen in the optical depth of H I 21-cm absorption towards different sightlines across the southern lobe (see Table 1). Again from the same table, we see that, while the gas shows no systematic velocity gradient over the region of the southern lobe, it does seem to have small-scale (few km s^{-1}) turbulent motion. We argue that it is this non-thermal motion that dominates the velocity spread (FWHM $\sim$8 km s^{-1}) of the absorption detected towards L2. In summary, the absorbing gas exhibits both large- (kpc) and small-scale (sub-kpc) structures, along with small-scale turbulent motion. Detailed understanding of the small-scale structures in the absorbing gas would greatly benefit from deeper H I 21-cm observations.

4.4 Metal absorption towards J0041−0143

Ca II and Na I absorption are detected towards the optical QSO J0041−0143 at z = 0.017721 in the Keck HIRES spectrum from the Keck Observatory Database of Ionized Absorbers toward Quasars (KODIAQ; O'Meara et al. 2015). We fit Voigt profiles to the metal

Table 1. Details of H I 21-cm absorption towards different radio sightlines of J0041−0143.

Sightline	Coordinates (J2000)	A_{L2} ($''$)	b_{L2} (kpc)	Peak Flux (mJy beam^{-1})	Spectral rms (mJy beam^{-1} channel^{-1})	τ_p	$\int \tau dv$ (km s^{-1})	log N(H I) (T_s/100 K)(1/f_c) (cm^{-2})	v_{L2} (km s^{-1})
(1)	(2)	(3)	(4)	(5)	(6)	(7)	(8)	(9)	(10)
Continuum peaks of the core and the lobes									
L1	00:41:26.11 −01:43:05.59	19.1	6.9	354.0	2.3	<0.01	<0.07	<19.10	—
C	00:41:26.01 −01:43:14.59	10.0	3.6	66.7	2.1	<0.03	<0.28	<19.71	—
L2	00:41:25.98 −01:43:24.59	0	0	215.1	2.1	0.08 ± 0.01	0.52 ± 0.07	19.98 ± 0.05	0
Locations in the southern lobe									
1	00:41:25.98 −01:43:22.59	2.0	0.7	96.3	2.5	0.09 ± 0.02	0.35 ± 0.16	19.80 ± 0.20	-3.6 ± 2.3
2	00:41:26.18 −01:43:24.09	3.0	1.1	37.9	2.3	0.19 ± 0.07	1.20 ± 0.42	20.34 ± 0.15	$+1.1 \pm 1.2$
3	00:41:25.78 −01:43:25.09	3.0	1.1	28.2	1.9	0.12 ± 0.06	1.14 ± 0.48	20.32 ± 0.18	$+4.6 \pm 1.3$
4	00:41:26.01 −01:43:20.59	4.0	1.5	45.6	2.1	0.13 ± 0.05	0.65 ± 0.33	20.07 ± 0.22	$+3.9 \pm 1.7$

Column 1: Radio sightline (as labelled in Figs. 1 and 4). Column 2: J2000 coordinates of the radio sightline. Columns 3 & 4: Angular (in arcsec) and projected (in kpc) separation at the redshift of UGC 00439 with respect to L2, respectively. Column 5: Peak continuum flux in mJy beam^{-1}. Column 6: Spectral rms in mJy beam^{-1} channel^{-1} at velocity resolution of 1.8 km s^{-1}. Column 7: Peak H I 21-cm optical depth or 1σ limit to it in case of non-detections. Column 8: Integrated H I 21-cm optical depth or 3σ upper limit in case of non-detections with data smoothed to 10 km s^{-1}. Column 9: log N(H I) (in cm^{-2}) corresponding to the optical depth given in column 8 for $T_s = 100$ K and $f_c = 1$. Column 10: Optical depth weighted mean velocity (in km s^{-1}), in case of detections, with respect to the velocity of peak optical depth detected towards L2.

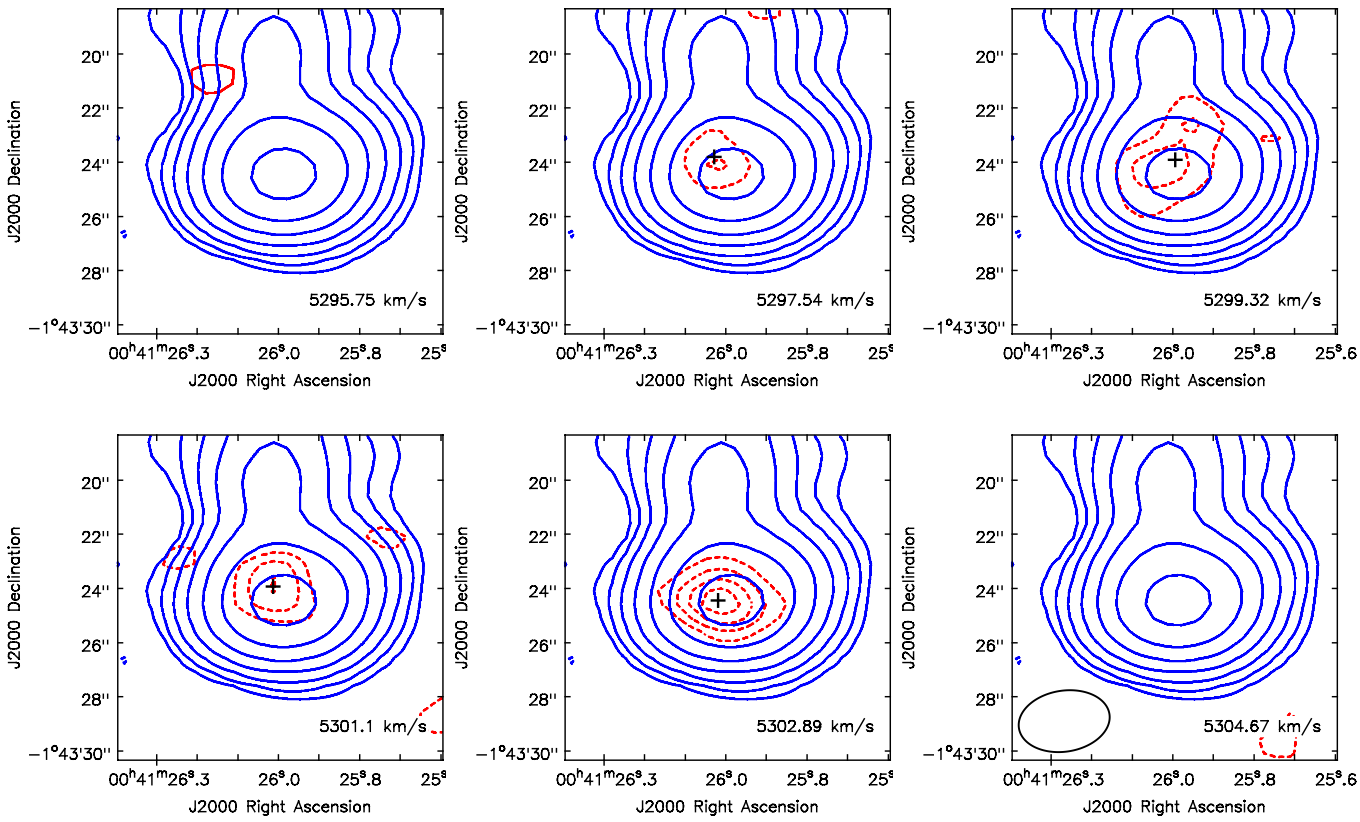

Figure 3. Channels maps of the H I 21-cm absorption towards J0041−0143 separated by 1.8 km s^{-1}. The blue contours and the beam are the same as in Fig. 1. The red contours show the H I 21-cm absorption with the levels plotted as 6.0 × (−2.5, −2.0, −1.5, −1.0, 1.0, 1.5, 2.0, 2.5) mJy beam^{-1} . The crosses mark the centre of the absorption obtained from two-dimensional single Gaussian fit. Note that solid lines correspond to positive values while dashed lines correspond to negative values. Heliocentric velocity of each channel is also given.

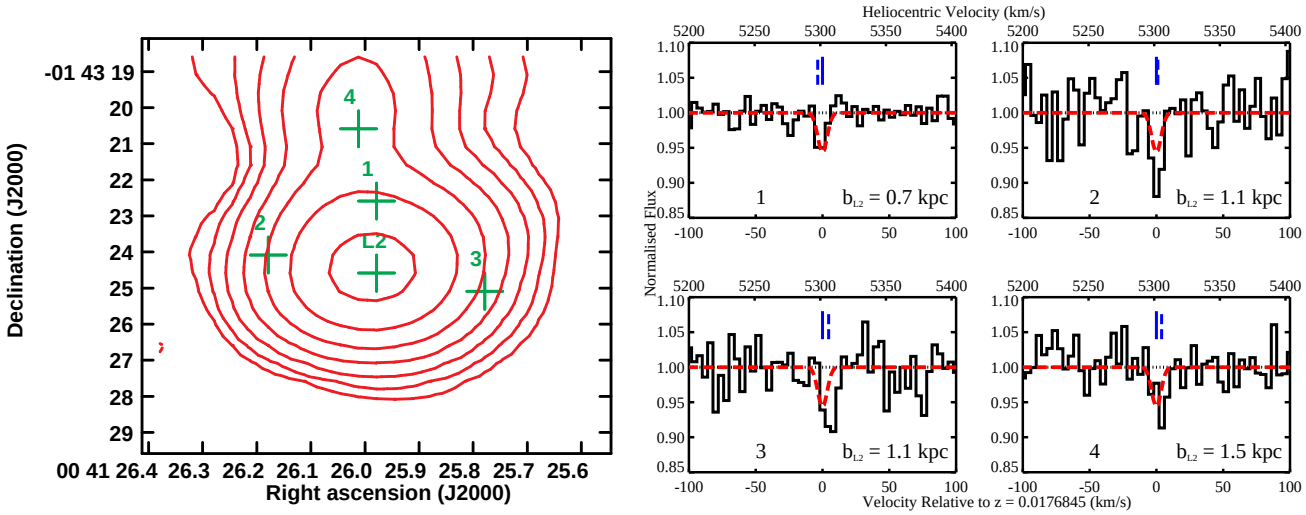

Figure 4. *Left:* The contours and the beam are the same as in Fig. 1 with the southern lobe zoomed in. Marked are the different sightlines, separated by the beam size, towards which H I 21-cm absorption spectra are extracted. *Right:* The GMRT H I 21-cm absorption spectra (smoothed to 4 km s^{-1} for display purpose) towards the sightlines 1, 2, 3 and 4 as marked in the figure to the left. Overplotted in dashed red line is the best-fitting Gaussian profile to the H I 21-cm absorption towards L2, as shown in the bottom panel of Fig. 2, for comparison. The vertical solid tick marks the position of the peak optical depth detected towards L2, while the dashed tick marks the position of the optical depth weighted mean velocity of the absorption. b_{L2} is as defined in Fig. 2. Details of the spectra extracted from different locations can be found in Table 1.

lines using VPFIT[2]. The best-fitting single component Voigt profile with Doppler parameter of 4.1 $\pm$ 0.3 km s^{-1} (or FWHM of 6.7 $\pm$ 0.5 km s^{-1}) gives log N(Ca II) = 12.40 $\pm$ 0.06 and log N(Na I) = 12.29 $\pm$ 0.03. In Fig. 5, we show the metal absorption and the best-fitting Voigt profiles. The metal absorption towards the optical QSO, which is cospatial with the radio core, indicates the presence of H I gas at this location. Moreover, since Ca II and Na I are usually believed to be tracers of cold gas, the H I gas detected in absorption towards L2 is likely to extend up to the core (with factor $\gtrsim$2 variation in optical depth). Note that the peak of the metal absorption is redshifted by $\sim$11 km s^{-1} with respect to the peak H I 21-cm optical depth towards L2. In other words, since the H I 21-cm absorption occurs at the systematic redshift of UGC 00439, the metal absorption is redshifted with respect to the systematic redshift of the host galaxy.

In the Galactic ISM, N(Na I)/N(Ca II) $>$ 1 for the observed values of N(Na I) (Welty et al. 1996, Fig. 9), while the observed ratio is $\sim$ 1 in the present case. This could mean that Ca depletion is not as high as that typically seen (~ -3 dex) in the Galactic ISM, and accordingly the N(H I) may not be very high since depletion usually correlates with it. If N(Na I) scales with N(H I) as seen in our Galaxy (Ferlet et al. 1985; Wakker & Mathis 2000), then we expect log N(H I) $\sim$20.6. In that case, from the H I 21-cm optical depth limit towards the core, the gas would have $T_s \gtrsim 800$ K (for f_c = 1). On the other hand, if we assume the gas to be cold ($\sim$100 K), we expect log N(H I) $<$19.7 (for f_c = 1; see Table 1), or $\gtrsim 8$ times more Na I per H I to be present in this gas than what is typically seen in the Galactic ISM. As Na I is not the dominant ion of Na in the H I phase, this can be explained by the ionizing field at the location of the absorber being weaker than the mean Galactic radiation field, as expected in the outer extended H I disc. Hence, Na I may not be a good tracer of H I in sightlines that pass away from the stellar disc of galaxies (e.g. Dutta et al. 2015).

[2] http://www.ast.cam.ac.uk/$\sim$rfc/vpfit.html

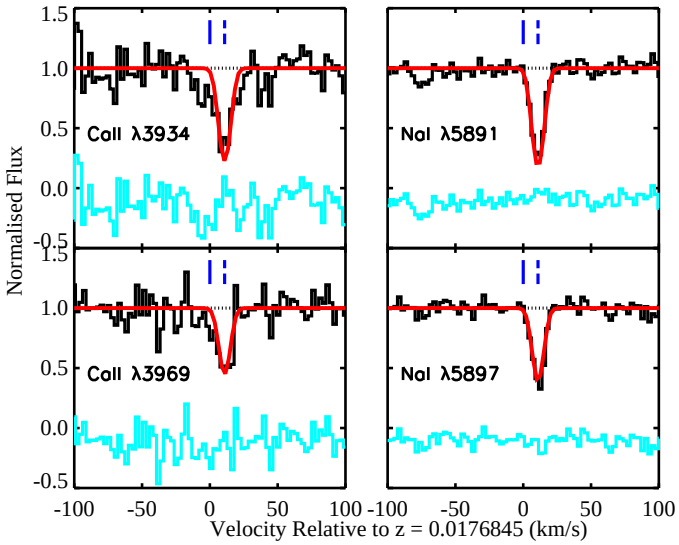

Figure 5. The Ca II and Na I absorption towards the QSO J0041−0143 detected in the Keck-HIRES spectrum. The optical emission of the QSO coincides with component C. Best-fitting Voigt profiles are overplotted in red. The residuals from the fit are shown at the bottom in cyan. The vertical solid and dashed ticks mark the positions of the peak H I 21-cm optical depth detected towards L2 and of the peak metal absorption respectively.

4.5 H I 21-cm emission from UGC 00439

In order to detect H I 21-cm emission from the galaxy using GMRT data, we imaged the continuum subtracted visibilities with different *uv*-tapers and robust weightings to make spectral cubes of different spatial resolutions. We find that the H I 21-cm emission can be best measured using the present data at a spatial resolution of $46.4'' \times 33.4''$ (i.e. 17 kpc $\times$ 12 kpc). A coarser spatial resolution does not lead to increase in the total flux density detected from the galaxy, and the present data do not have sufficient signal-to-noise ratio to detect H I 21-cm emission reliably at a finer spa-

tial resolution. Hence, the discussion on H I 21-cm emission presented in this paper is based on the image cube of spatial resolution $46.4'' \times 33.4''$ and velocity resolution $\sim$7.1 km s^{-1}, made using `ROBUST=1` weighting (rms $\sim$2 mJy beam^{-1} channel^{-1}). While imaging, the H I 21-cm emission signal was deconvolved using mask(s) true only for pixels with absolute flux > 3 times the single channel rms. The global H I 21-cm emission spectrum is obtained from this cube by integrating the flux density over all the regions where H I 21-cm emission associated with UGC 00439 is detected. The total integrated flux density of the H I 21-cm emission is, $\int Sdv = 1.42 \pm 0.14$ Jy km s^{-1}. The GMRT H I 21-cm emission is detected over almost the full velocity range of the Arecibo emission, with the double peaks of the emission profiles matching in velocity (see Fig. 6 for comparison). Note that the total GMRT H I 21-cm emission recovers only $\sim$20% of that found in the Arecibo spectrum. However, the flux recovered in the wings and the two peaks is $\sim$33% of that in the Arecibo profile, i.e. there is no uniform offset in amplitude between the two profiles. This implies that the H I 21-cm emission that is not detected by the GMRT data could be arising from a separate component of the H I gas associated with UGC 00439. The poor sensitivity and *uv*-coverage of the GMRT data perhaps does not allow us to detect any diffuse and extended H I gas around UGC 00439. We discuss the structure and kinematics of the H I gas associated with UGC 00439 further in Section 5.1.

For generating H I 21-cm moments maps, we made a mask based on emission detected above a threshold of 3σ noise in the original image cube and the cube smoothed over twice the spatial and the velocity resolution. We show the contours of the total H I 21-cm (moment-0) map, corrected for the primary beam attenuation, overlaid on the SDSS r-band image in the left-hand panel of Fig. 7, with the outermost level corresponding to log N(H I) = 19.6, and the highest density clumps corresponding to log N(H I) = 20.4. We can see that the H I 21-cm emission, detected in the GMRT data, extends beyond the optical disc of the galaxy, but does not extend up to the QSO, J0041$-$0143. We also checked in the channel maps of the cube which contain the H I 21-cm absorption, that no H I 21-cm emission extends up to the location of the absorber. The moment-1 map showing the H I 21-cm velocity field is shown in the right-hand panel of Fig. 7. It shows that the H I 21-cm emission exhibits clear signs of rotation. We discuss the implications of the H I 21-cm observations on the extended H I disc of the galaxy and the H I 21-cm absorber in the next section.

5 DISCUSSION

5.1 Structure and kinematics of the H I gas associated with UGC 00439

The double-peaked H I 21-cm emission in the Arecibo as well as the GMRT spectra indicate that the H I disc is rotating at an inclination to the line of sight. We find that a simple rotating disc galaxy model following Schulman et al. (1994), with i = 30° and maximum velocity of 110 km s^{-1} can reproduce the velocity separation between the two horns of the H I 21-cm emission reasonably well (see Fig. 6). While the galactic disc is inferred to have a zero inclination in the optical bands, the H I disc inclination from the model is consistent with the inclination inferred in the 2MASS infrared K_s band, which is expected to trace the old stellar population unbiased by dust. By comparing the GMRT moment-1 map and the SDSS image of UGC 00439 in Fig. 7, we can see that the H I 21-cm emission on the northern (southern) part of the galaxy

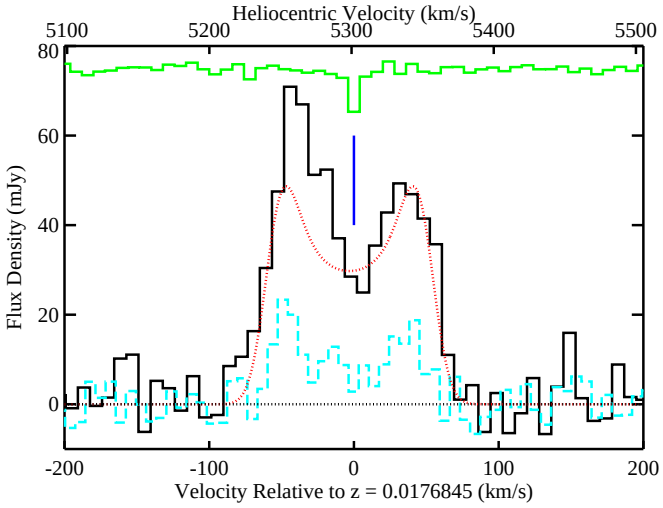

Figure 6. The Arecibo H I 21-cm emission spectrum (Springob et al. 2005) in solid histogram and the GMRT H I 21-cm emission spectrum in dashed histogram of the galaxy, UGC 00439. The H I 21-cm emission spectrum expected from a simple rotating disc galaxy model (see Section 5.1 for details) is overplotted in dotted line. Shown in green is the H I 21-cm absorption spectrum towards L2, smoothed to the velocity resolution of the Arecibo spectrum ($\sim$8 km s^{-1}), and offset by 75 mJy along the y-axis for ease of comparison. The vertical tick marks the location of the peak optical depth found in the H I 21-cm absorption spectrum.

is redshifted (blueshifted) with respect to the systematic velocity. Based on the limited H I 21-cm data, the kinematical major axis of the H I 21-cm emission seems to lie along that of the optical and the infrared emission (PA = 160$-$170°). Additionally, we note that there is excess H I 21-cm emission in the extreme blue wing of the Arecibo H I 21-cm profile (~ -80 km s^{-1}) that cannot be explained by a simple rotating disc model. Excess emission in the wings have been explained by high velocity clouds as seen in our Galaxy or a warped H I disc (Schulman et al. 1994). Deeper H I 21-cm emission observations are required to derive the distribution and kinematics of H I gas in UGC 00439, and distinguish between these scenarios.

Further, from Fig. 6, the Arecibo H I 21-cm emission is asymmetric in amplitude with respect to the systematic velocity of the galaxy, with $\sim$20% more flux in the blue side. This asymmetry is also present to a lesser extent in the GMRT H I 21-cm emission. It can be seen from Fig. 7, that the H I 21-cm emission on the southern side of the galaxy, which corresponds to the blue peak, seems to be more extended than the emission on the northern part, corresponding to the red peak. Asymmetry in the global H I 21-cm profile can be traced to asymmetry in the H I gas distribution along with that in the disc kinematics. We find that even in the available UV and infrared images of this galaxy, the stellar disc seems to be asymmetric in terms of its spiral structure and light distribution, reflecting the asymmetry evident in the H I gas distribution. Richter & Sancisi (1994), from the frequency of lopsided H I 21-cm profiles, derive a lower limit of 50% for the fraction of galaxies with non-circular density distribution. Such lopsidedness may arise out of accretion or merger events in the past.

Since UGC 00439 is part of a galaxy group (see Fig. 8), this is certainly a possibility. The structure and kinematics of the extended H I disc are known to be highly affected by interaction/merger events, and in few cases the highest density H I has been observed to be beyond the optical discs (e.g. Hibbard & van Gorkom 1996; Duc et al. 1997; Sengupta et al. 2013, 2015). In the GMRT

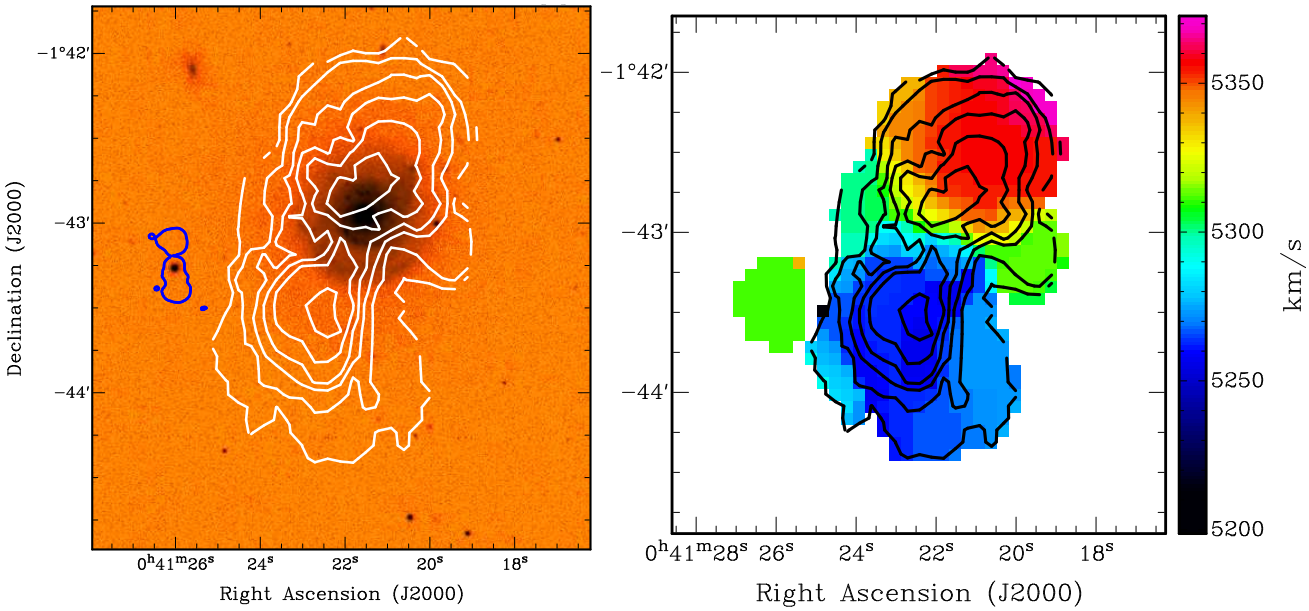

Figure 7. *Left:* SDSS r-band image of the QGP, J0041−0143/UGC 00439, is shown. The GMRT H I 21-cm moment-0 map (of spatial resolution $46.4'' \times 33.4''$) is shown as a contour plot, with the levels corresponding to N(H I) = (0.4, 0.8, 1.2, 1.6, 2.0, 2.4) $\times$ 10^{20} cm^{-2}. The outermost contour of the GMRT radio continuum of J0041−0143 from Fig. 1 (2.5 mJy beam^{-1}) is also shown for reference in blue. *Right:* The GMRT moment-1 map of UGC 00439 overlaid with contours of the moment-0 map as shown to the left. The green patch at the location of the quasar corresponds to the redshift of the H I 21-cm absorption. Note that from Arecibo H I 21-cm measurement, UGC 00439 has V_H = 5302 $\pm$ 2 km s^{-1}.

data, we detect H I 21-cm emission from two other galaxies at b ∼150 kpc from UGC 00439 in the group (see also Fig. 8): UGC 00435 (J004059.6−013802; z = 0.018139; V_H = 5438 km s^{-1}) and CGCG 383−072 (J004148.4−01441; z = 0.018356; V_H = 5503 km s^{-1}). For the former we measure $\int Sdv$ = 0.52 $\pm$ 0.15 Jy km s^{-1}, and for the latter $\int Sdv$ = 0.76 $\pm$ 0.20 Jy km s^{-1}. UGC 00435 has been studied in H I 21-cm emission using Nancay by Theureau et al. (2007), who gives $\int Sdv = 2.57 \pm 0.47$ Jy km s^{-1}. The GMRT data recovers ∼20% of the single dish measurement of this galaxy.

5.2 Connecting the H I 21-cm absorber with the host galaxy

The H I 21-cm absorption occurs at the systematic velocity of the galaxy, as evident from Fig. 6, which shows that the peak H I 21-cm absorption towards L2 coincides with the centre of the H I 21-cm emission. This indicates that the absorber is located along the kinematic minor axis of the H I disc. Moreover, the absorption is narrow and shows no signatures of outflowing/infalling gas. Hence, the gas detected in H I 21-cm absorption is most likely to follow the rotation of the extended H I disc of the galaxy. Recall from Section 4.3 that the H I 21-cm absorbing gas shows no systematic velocity gradient over the region (∼2 kpc^{-2}) of the southern lobe of J0041−0143. But as mentioned in Section 4.4 and shown in Fig. 5, the metal absorption detected towards the core (∼4 kpc north of the southern lobe) is redshifted by ∼11 km s^{-1} with respect to the H I 21-cm absorption. We estimate the expected velocity shift due to rotation with respect to the systematic velocity of the galaxy as ∼7 km s^{-1} at the location of the core (using the maximum rotational velocity from the Arecibo H I 21-cm emission and the PAs of L2 and C). Hence, both the H I 21-cm and the metal absorption could be tracing gas that is corotating with the H I disc.

In most of the low-z QGPs in which H I 21-cm absorption has been detected in literature, the radio sightline passes through either the stellar disc or the extended H I disc of the foreground galaxy (b <20 kpc, Gupta et al. 2013; Zwaan et al. 2015). On the other hand, impact parameters of host galaxy candidates of low-z H_2 absorbers have been found to be much further away from the stellar disc (10$\lesssim$ b(kpc)$\lesssim$80, Muzahid et al. 2015). The authors conjecture that the H_2 bearing gas may stem from self-shielded, tidally stripped or ejected disc-material in the extended galactic halo. In the present case, since the H I 21-cm absorber is detected away from the optical/UV QSO sightline, we can clearly see that there is no indication of star formation (i.e. no stellar light) at the location of the H I 21-cm absorber in the available optical and UV images (see e.g. the SDSS r-band image in Fig. 7). We estimate m_r = 21.9 and m_{NUV} = 22.5 in a circular aperture of 5″ placed over the southern lobe in the SDSS r-band and GALEX near-UV images respectively. This suggests that the absorption is unlikely to arise from the ISM of a low-luminosity dwarf galaxy at that location. Hence, this supports our above conjecture that we are most likely tracing clumps of corotating cold gas in the extended H I disc of the galaxy.

We note that better sensitivity H I 21-cm emission maps of the extended H I gas distribution around the galaxy are required to quantify the physical conditions in the absorbing gas. However, we can draw some simple estimates of the physical conditions in the absorbing gas using the N(H I) sensitivity of the GMRT data across different spatial scales. As described in Section 4.5, we constructed image cubes of different spatial resolutions in order to detect H I 21-cm emission. In Fig. 9, we show the N(H I) sensitivity (at 3 and 5 σ significance) per velocity channel (7.1 km s^{-1}) for different spatial resolutions, estimated using the rms in line-free channels in these image cubes. Note that the H I 21-cm absorption is spread over only one channel at the velocity resolution in these cubes. The horizontal line marks the log N(H I) we expect to be associated with the absorbing gas towards L2 if it has T_s = 100 K and f_c = 1 (see Table 1). H I 21-cm emission is not detected at the location of the H I

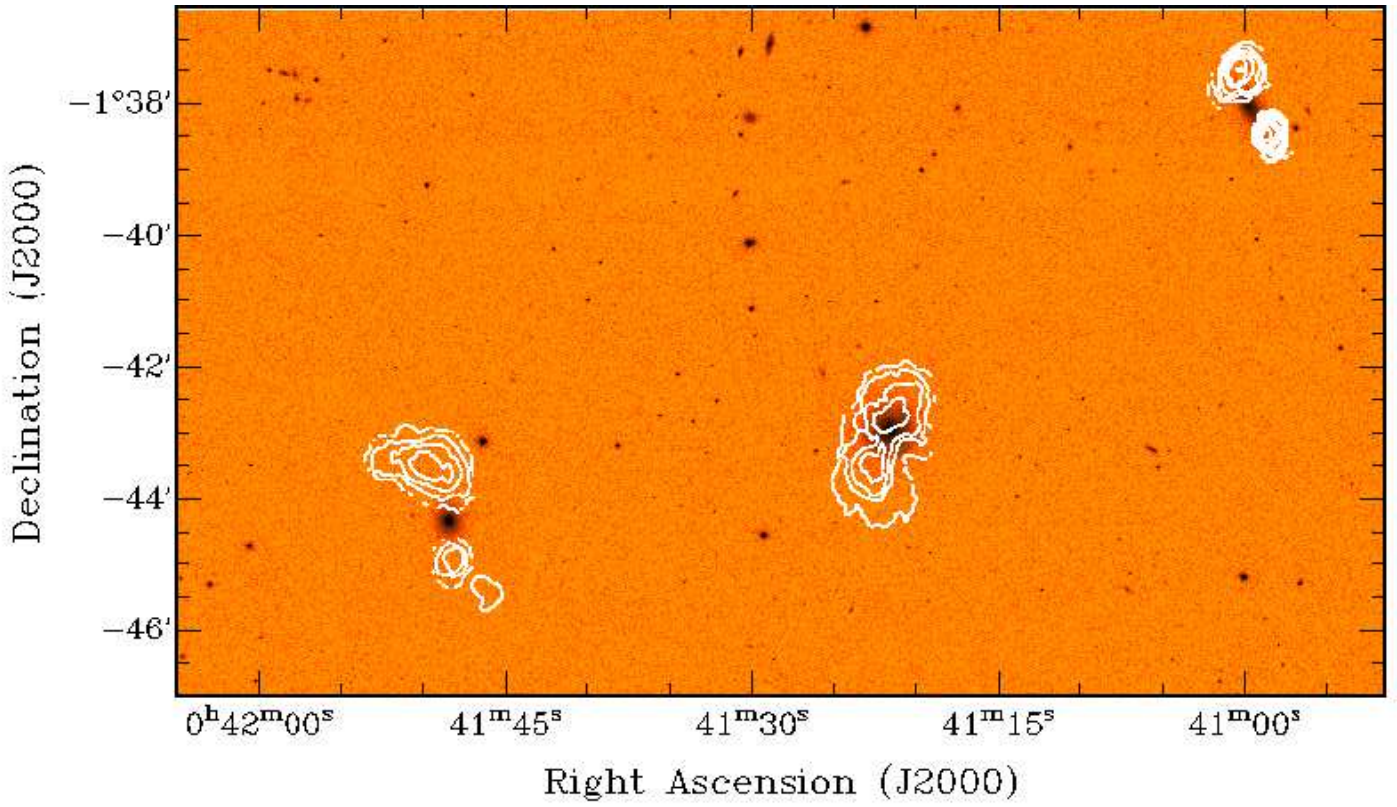

Figure 8. SDSS r-band image of the field around UGC 00439 overlaid with contours of the GMRT moment-0 map. The contour levels correspond to N(H I) = (0.4, 1.0, 1.6,...) $\times$ 10^{20} cm^{-2}. H I 21-cm emission is detected from two other galaxies at 7′ ($\sim$150 kpc) from UGC 00439 in the GMRT field of view: UGC 00435 (J004059.6−013802; z = 0.018139; V_H = 5438 km s^{-1}) and CGCG 383−072 (J004148.4−01441; z = 0.018356; V_H = 5503 km s^{-1}).

21-cm absorption in the image cubes with a resolution of $\geqslant$10 kpc, where we have sufficient sensitivity to detect up to typical N(H I) seen in sub-damped Lyman-α systems (N(H I) $\geqslant$ 10^{19} cm^{-2}; see Wolfe et al. 1982, 2005; Péroux et al. 2005). This implies that either the absorbing gas, spread over $\geqslant$10 kpc, has temperature less than 100 K, or that the cold $\sim$100 K gas is more compact than $\sim$10 kpc. In Section 4.3, we saw that the absorbing gas extends up to at least 1 kpc and may extend up to $\sim$4 kpc with optical depth varying by a factor of $\gtrsim$2. The present data does not have sufficient sensitivity to detect cold 100 K gas of size $\sim$4 kpc. However, from the non-detection of H I 21-cm emission over this scale we get a limit on the temperature of the absorbing gas as $\lesssim$300 K.

The fact that the H I 21-cm optical depth falls by a factor of $\gtrsim$7 over $\sim$7 kpc at similar impact parameters from the galaxy could be a manifestation of patchy distribution of cold gas in the extended H I disc, with a varying covering factor at different spatial locations. This variation in optical depth at similar radius from the galaxy should be taken into account when interpreting the covering factor of H I 21-cm absorbers around low-z galaxies.

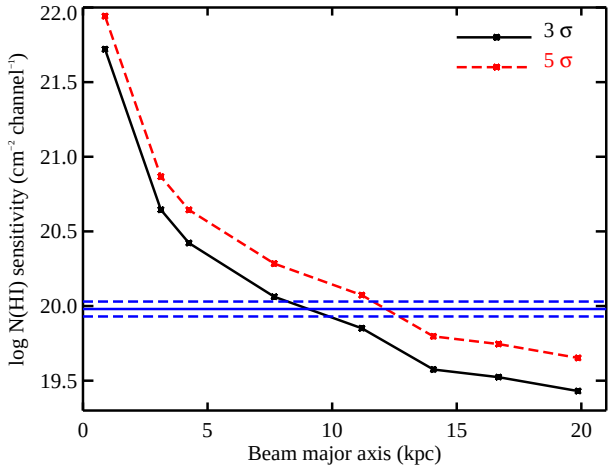

Figure 9. The 3σ (5σ) N(H I) sensitivity per channel (7.1 km s^{-1}) at different spatial resolutions, in the GMRT H I 21-cm emission data set, is shown as a solid (dashed) line. The horizontal solid line marks the log N(H I) corresponding to the optical depth detected towards L2 for a 100 K gas with f_c = 1 (see Table 1), and the dashed horizontal lines show the 1σ errors associated with it.

6 SUMMARY

This paper presents GMRT H I 21-cm absorption and emission observations of the QGP, J0041−0143/UGC 00439. The background radio source consists of a core component and two lobes, all at a projected separation of $\sim$25 kpc from the z = 0.01769 galaxy, UGC 00439. We detect H I 21-cm absorption towards the southern lobe but not towards the core ($\sim$4 kpc north of southern lobe) or the northern lobe ($\sim$7 kpc north of southern lobe). The H I 21-cm absorption towards the continuum peak of the southern lobe corresponds to an integrated optical depth of 0.52 $\pm$ 0.07 km s^{-1} and a FWHM of 8 $\pm$ 1 km s^{-1}. From channel maps of the absorption and spatially resolved extraction of H I 21-cm spectra over the southern

lobe, we surmise that the absorbing gas is likely to have sub-kpc structures and turbulent motion of the order of few km s^{-1}, extending over a $\sim$2 kpc^2 region. The absorbing gas may extend up to the core, which is cospatial with the optical QSO and towards which we detect Ca II and Na I absorption in the Keck-HIRES spectrum.

The GMRT H I 21-cm emission associated with UGC 00439 recovers $\sim$20% of the total flux density measured by Arecibo. The Arecibo and GMRT H I 21-cm observations of this galaxy suggest that its H I disc is lopsided, which may arise out of interaction/merger events. Detection of H I 21-cm emission from two other neighbouring galaxies, $\sim$150 kpc away from UGC 00439, in the GMRT data, gives credence to the idea that some of the H I gas in UGC 00439 may have been stripped out of its regular rotating disc due to tidal interactions with neighbouring galaxies. From the N(H I) sensitivity of the GMRT observations at different spatial scales, we estimate that if the absorber had a spatial extent of $\sim$4 kpc, its temperature would be $\lesssim$300 K. Further, the H I 21-cm absorption arises at the systematic redshift of the galaxy, with no stellar light detected at its location, implying that it is most likely tracing clumpy gas corotating with the H I disc of the galaxy.

The GMRT observations reveal kpc to sub-kpc structures in the H I gas around UGC 00439. However, it still leaves some questions regarding the nature of the H I gas unanswered. A higher sensitivity H I 21-cm emission map is required to study the H I gas distribution at the location of the background radio source. Further, subarcsecond-scale radio observations of J0041$-$0143 will help in quantifying the covering factor and parsec-scale structures in the absorbing gas. In addition, two-dimensional optical spectra of UGC 00439 along with deeper H I 21-cm observations would help to better compare the distribution and kinematics of the stellar population and the H I gas. Lastly, higher sensitivity H I 21-cm emission observations would help to map any large-scale diffuse H I gas that may exist as a result of tidal interactions/mergers between the nearby galaxies.

Hence, while the results presented in this paper help in characterizing the H I gas around UGC 00439, they also motivate future observations of this system. In addition, the results presented in this paper along with our ongoing study of H I 21-cm absorption in the discs/haloes of low-z galaxies (Gupta et al. 2010, 2013; Srianand et al. 2013, 2015, Dutta et al. in preparation), are expected to establish the elusive link between H I 21-cm absorbers and host galaxy properties, and play a vital role in understanding the nature of high-z H I 21-cm absorbers (Briggs & Wolfe 1983; Kanekar & Chengalur 2003; Curran et al. 2005; Gupta et al. 2009, 2012; Srianand et al. 2012; Kanekar et al. 2014), as well as the large number of H I 21-cm absorbers expected to be detected from upcoming blind surveys (e.g. MeerKAT Absorption Line Survey) using Square Kilometre Array pathfinders and precursors.

ACKNOWLEDGEMENTS

We thank the anonymous referee for his/her useful comments. We thank the GMRT staff for their help during the observations. GMRT is run by the National Centre for Radio Astrophysics of the Tata Institute of Fundamental Research. Some of the data presented in this work were obtained from the Keck Observatory Database of Ionized Absorbers toward Quasars (KODIAQ), which was funded through NASA ADAP grant NNX10AE84G.

REFERENCES

Bagetakos, I., Brinks, E., Walter, F., de Blok, W. J. G., Usero, A., Leroy, A. K., Rich, J. W., & Kennicutt, Jr., R. C., 2011, AJ, 141, 23
Barthel, P. D., Miley, G. K., Schilizzi, R. T., & Lonsdale, C. J., 1988, A&AS, 73, 515
Borthakur, S., Tripp, T. M., Yun, M. S., Bowen, D. V., Meiring, J. D., York, D. G., & Momjian, E., 2011, ApJ, 727, 52
Borthakur, S., Tripp, T. M., Yun, M. S., Momjian, E., Meiring, J. D., Bowen, D. V., & York, D. G., 2010, ApJ, 713, 131
Briggs, F. H., de Bruyn, A. G., & Vermeulen, R. C., 2001, A&A, 373, 113
Briggs, F. H. & Wolfe, A. M., 1983, ApJ, 268, 76
Broeils, A. H. & Rhee, M.-H., 1997, A&A, 324, 877
Brogan, C. L., Zauderer, B. A., Lazio, T. J., Goss, W. M., DePree, C. G., & Faison, M. D., 2005, AJ, 130, 698
Carilli, C. L. & van Gorkom, J. H., 1992, ApJ, 399, 373
Curran, S. J., Murphy, M. T., Pihlström, Y. M., Webb, J. K., & Purcell, C. R., 2005, MNRAS, 356, 1509
de Avillez, M. A. & Breitschwerdt, D., 2004, A&A, 425, 899
Deshpande, A. A., 2000, MNRAS, 317, 199
Downes, A. J. B., Peacock, J. A., Savage, A., & Carrie, D. R., 1986, MNRAS, 218, 31
Duc, P.-A., Brinks, E., Wink, J. E., & Mirabel, I. F., 1997, A&A, 326, 537
Dutta, R., Srianand, R., Muzahid, S., Gupta, N., Momjian, E., & Charlton, J., 2015, MNRAS, 448, 3718
Ferlet, R., Vidal-Madjar, A., & Gry, C., 1985, ApJ, 298, 838
Fernini, I., 2014, ApJS, 212, 19
Frail, D. A., Weisberg, J. M., Cordes, J. M., & Mathers, C., 1994, ApJ, 436, 144
Gatto, A., Walch, S., Low, M.-M. M., et al., 2015, MNRAS, 449, 1057
Gent, F. A., Shukurov, A., Fletcher, A., Sarson, G. R., & Mantere, M. J., 2013, MNRAS, 432, 1396
Gupta, N., Srianand, R., Bowen, D. V., York, D. G., & Wadadekar, Y., 2010, MNRAS, 408, 849
Gupta, N., Srianand, R., Noterdaeme, P., Petitjean, P., & Muzahid, S., 2013, A&A, 558, A84
Gupta, N., Srianand, R., Petitjean, P., Bergeron, J., Noterdaeme, P., & Muzahid, S., 2012, A&A, 544, A21
Gupta, N., Srianand, R., Petitjean, P., Noterdaeme, P., & Saikia, D. J., 2009, MNRAS, 398, 201
Heiles, C., 1984, ApJS, 55, 585
Heiles, C. & Troland, T. H., 2003, ApJ, 586, 1067
Hibbard, J. E. & van Gorkom, J. H., 1996, AJ, 111, 655
Huang, S., Haynes, M. P., Giovanelli, R., & Brinchmann, J., 2012, ApJ, 756, 113
Ianjamasimanana, R., de Blok, W. J. G., Walter, F., & Heald, G. H., 2012, AJ, 144, 96
Jansen, R. A., Fabricant, D., Franx, M., & Caldwell, N., 2000a, ApJS, 126, 331
Jansen, R. A., Franx, M., Fabricant, D., & Caldwell, N., 2000b, ApJS, 126, 271
Jones, D. H., Read, M. A., Saunders, W., et al., 2009, MNRAS, 399, 683
Kanekar, N. & Chengalur, J. N., 2001, MNRAS, 325, 631
—, 2003, A&A, 399, 857
—, 2005, in IAU Colloq. 199: Probing Galaxies through Quasar Absorption Lines, Williams, P., Shu, C.-G., & Menard, B., eds., pp. 156–161

Kanekar, N., Prochaska, J. X., Smette, A., et al., 2014, MNRAS, 438, 2131
Kannappan, S. J., Stark, D. V., Eckert, K. D., et al., 2013, ApJ, 777, 42
Keeney, B. A., Momjian, E., Stocke, J. T., Carilli, C. L., & Tumlinson, J., 2005, ApJ, 622, 267
Keeney, B. A., Stocke, J. T., Danforth, C. W., & Carilli, C. L., 2011, AJ, 141, 66
Kewley, L. J., Geller, M. J., & Jansen, R. A., 2004, AJ, 127, 2002
Lah, P., Pracy, M. B., Chengalur, J. N., et al., 2009, MNRAS, 399, 1447
McKee, C. F. & Ostriker, J. P., 1977, ApJ, 218, 148
Muzahid, S., Srianand, R., & Charlton, J., 2015, MNRAS, 448, 2840
O'Meara, J. M., Lehner, N., Howk, J. C., et al., 2015, AJ, 150, 111
Péroux, C., Dessauges-Zavadsky, M., D'Odorico, S., Sun Kim, T., & McMahon, R. G., 2005, MNRAS, 363, 479
Reeves, S. N., Sadler, E. M., Allison, J. R., Koribalski, B. S., Curran, S. J., & Pracy, M. B., 2015, MNRAS, 450, 926
Richter, O.-G. & Sancisi, R., 1994, A&A, 290, L9
Roy, N., Chengalur, J. N., & Srianand, R., 2006, MNRAS, 365, L1
Schulman, E., Bregman, J. N., & Roberts, M. S., 1994, ApJ, 423, 180
Sengupta, C., Dwarakanath, K. S., Saikia, D. J., & Scott, T. C., 2013, MNRAS, 431, L1
Sengupta, C., Scott, T. C., Paudel, S., Saikia, D. J., Dwarakanath, K. S., & Sohn, B. W., 2015, A&A, 584, A114
Skrutskie, M. F., Cutri, R. M., Stiening, R., et al., 2006, AJ, 131, 1163
Springob, C. M., Haynes, M. P., Giovanelli, R., & Kent, B. R., 2005, ApJS, 160, 149
Srianand, R., Gupta, N., Momjian, E., & Vivek, M., 2015, MNRAS, 451, 917
Srianand, R., Gupta, N., Petitjean, P., Noterdaeme, P., Ledoux, C., Salter, C. J., & Saikia, D. J., 2012, MNRAS, 421, 651
Srianand, R., Gupta, N., Rahmani, H., Momjian, E., Petitjean, P., & Noterdaeme, P., 2013, MNRAS, 428, 2198
Stocke, J. T., Case, J., Donahue, M., Shull, J. M., & Snow, T. P., 1991, ApJ, 374, 72
Stocke, J. T., Keeney, B. A., & Danforth, C. W., 2010, PASA, 27, 256
Tamburro, D., Rix, H.-W., Leroy, A. K., Mac Low, M.-M., Walter, F., Kennicutt, R. C., Brinks, E., & de Blok, W. J. G., 2009, AJ, 137, 4424
Theureau, G., Hanski, M. O., Coudreau, N., Hallet, N., & Martin, J.-M., 2007, A&A, 465, 71
Wakker, B. P. & Mathis, J. S., 2000, ApJ, 544, L107
Welty, D. E., Morton, D. C., & Hobbs, L. M., 1996, ApJS, 106, 533
Wolfe, A. M., Briggs, F. H., & Davis, M. M., 1982, ApJ, 259, 495
Wolfe, A. M., Gawiser, E., & Prochaska, J. X., 2005, ARA&A, 43, 861
Wolfire, M. G., Hollenbach, D., McKee, C. F., Tielens, A. G. G. M., & Bakes, E. L. O., 1995, ApJ, 443, 152
Zwaan, M. A., Liske, J., Péroux, C., Murphy, M. T., Bouché, N., Curran, S. J., & Biggs, A. D., 2015, MNRAS, 453, 1268